# Time Stretching of the GeV Emission of GRBs: Fermi LAT data vs geometrical model

Maxim S. Piskunov[1]*and Grigory I. Rubtsov[1]†
[1]Institute for Nuclear Research RAS, 117312, Moscow, Russia

January 18, 2014

**Abstract**

Numerous observations confirm that the high energy ($> 100\,\mathrm{MeV}$) emission of gamma ray bursts is delayed with respect to the low energy emission. However, the difference of light curves in various high energy bands has not been studied properly.

In this paper we consider all the bursts observed by Fermi-LAT since 2008 August 4 to 2011 August 1, for which at least 10 events with energies 1 GeV or higher were observed. There are 3 of them: GRB080916C, GRB090902B, and GRB090926A. We study their light curves in two bands, $(100\,\mathrm{MeV}, 1\,\mathrm{GeV})$ and $(1\,\mathrm{GeV}, 300\,\mathrm{GeV})$. The Kolmogorov-Smirnov test is used to check whether the light curves for these two bands are the same. No significant difference was found for GRB080916C and GRB090902B. However, we observed with statistical significance of $3.4\sigma$, that the higher energy light curve of GRB090926A is stretched with respect to the lower-energy one.

We suggest a simple geometrical model to explain this result. The main assumption is the jet opening angle dependence on radiation energy – the most energetic photons are emitted near the axis of the jet. To test this model, we compute the total energy of the burst, and confirm that it is below the constraint. We also compute the fraction of observable bursts in $(100\,\mathrm{MeV}, 1\,\mathrm{GeV})$ band, which can also be observed in higher energies. This fraction matches the observations. Finally, we predict the distribution of observable stretching factors, which may be tested in the future when more observational data will be available.

## 1 Introduction

Gamma Ray Bursts (GRBs) are among the most energetic events in the Universe, therefore they might provide new knowledge for particle physics. Recent observatories, specifically Fermi [Fermi-LAT12] and Swift [Science04] allowed for extensive study of these explosions [Via13, GR13]. These and previous studies led to several interesting results. For example, the total energy emitted in gamma-rays during a burst was found to be similar among different bursts within an order of magnitude [BFK03]. This suggests that most of the bursts must have similar energetics in their rest frame. Temporal variations of spectra were also studied. The spectral lags were found between different low energy bands [YLQL06]. The very high energy radiation was discovered to be extended if compared to x-ray emission [Via13, LP13]. Moreover, the Large Area Telescope (LAT) of Fermi allows us to explore the spectral variations even between high energy bands like $(100\,\mathrm{MeV}, 1\,\mathrm{GeV})$ and $(1\,\mathrm{GeV}, 300\,\mathrm{GeV})$ (we'll call them low and high energy bands). In this paper we use the Kolmogorov-Smirnov test to compute the time stretching of radiation in one of these bands compared to the other.

We take the GRB list from the Fermi-LAT catalog [AAA+13]. Tables 2 and 4 in [AAA+13] provide the time, durations and locations of the bursts, which we use to download events data from the LAT Data Server[1]. We also download events during a long time interval before the burst, and use the technique

*maxit@ms2.inr.ac.ru
†grisha@ms2.inr.ac.ru
[1]`http://fermi.gsfc.nasa.gov/cgi-bin/ssc/LAT/LATDataQuery.cgi`

introduced in [RPT12] to estimate background radiation in both energy bands. Most of the bursts in the catalog, however, do not have enough events with over 1 GeV energies to do desired computations, so we choose only those bursts for study, for which at least 10 photons were detected in the high energy band. This leaves 3 of them: 080916C [FLG09], 090902B [FS09] and 090926A [Fermi11].

For these 3 bursts we compute both high and low energy distributions of photon times. We subtract the low energy background estimate from the low energy CDF, and add the high energy background estimate to it. This makes the low energy CDF non-monotonous and, rigorously speaking, we cannot use the 2-sample Kolmogorov-Smirnov test on it. However, since there is a much greater number of photons on lower energies, we can think of the low energy CDF as continuous. Therefore, this non-monotonicity will be negligible, and will not harm the KS-test results much.

Finally, we stretch the high energy CDF by different factors, and compare it to the low energy CDF using the KS-test. If we require $2\sigma$-significant probability to exclude a particular stretching factor, then the stretching factor of 1 (which means no stretching) is allowed for GRBs 080916C and 090902B. However, for 090926A, the high energy light curve should be stretched with respect to the low energy one.

We propose that this result can be explained by the curvature effects (that is the effects of the jet geometry). These effects were explored by multiple authors [NI01, SSL05, SSD$^+$13]. However, these studies were only concerned with x-ray radiation, and, more importantly, they assumed that the distribution of radiation sources is homogeneous throughout the jet. We propose a contrary idea: that the highest energy radiators are concentrated near the axis of the burst, that is the burst opening angle depends on energy. We cannot prove this assumption rigorously, but we have arguments supporting it.

First of all, there are around 750 GRBs detected by GBM, half of which were in the LAT field of view [Via13]. However, only about 30 of them were detected by the LAT, and only 3 of them were bright in the high energy band. If we extrapolate the uniform jet model to very high energies, it means that these groups of bursts are internally different: some of them produce VHE radiation, and other do not. These differences are hard to explain given that burst energetics are similar [BFK03]. Nevertheless, these differences in burst counts can easily be explained by our model. In our model, the opening angle of low energy jet is much larger than the opening angle of a high energy jet. Therefore the most common scenario for an observable jet is that the off-axis angle of the observer is smaller than low energy jet opening angle, but larger than the opening angle of a high energy jet. Because of that, most of the bursts are only seen at low energies. The 3 bursts we study in this paper were seen from the lowest off-axis angles.

Secondly, consider the jet plasma right after emission from the central engine. There, two processes happen simultaneously:

1. Plasma particles near the jet boundary change directions, therefore increasing the jet opening angle.

2. Plasma particles lose energy, therefore decreasing radiation frequency emitted from the jet.

We argue that these two processes are correlated, because they happen due to the same particle interaction processes. And since they are correlated, jets with large opening angles will have lower energies, which is our main assumption.

Finally, this assumption is able to explain the non-trivial stretching factor of the GRB 090926A. The detailed computations will be described in the following sections, but you can see why the stretching is happening on the figure 1. The computations confirm that this qualitative picture is indeed correct, you can see a sample light curve on the figure 2, and predicted distribution of stretching factors on the figure 3.

# 2 Observations

## 2.1 Download and Process

## 2.2 Linear Component (background)

## 2.3 KS-test

## 2.4 Results

# 3 Model

## 3.1 Assumptions

To understand the observed spectral lag, lets explore geometry of the jet. First of all, lets make some assumptions:

1. Time $t = 0$, a spherical shell of plasma is emitted. The center is called the central engine.
2. The shell points propagate with a constant velocity $v \sim 1$, so at the time $t$ the radius of the shall is $vt$.
3. Each point of the shell is an isotropic radiator in its rest frame.
4. The radiation intensity is a function of the radiator position and the radiation frequency:

$$\eta\left(r,\theta,\omega\right) = \frac{\eta_0}{1+\left(\frac{r}{r_0}\right)^n} \exp\left(-\left(\frac{\theta}{\theta_0}\right)^2 \left(\frac{\omega}{\omega_0}\right)^{-2k}\right) \left(\frac{\omega}{\omega_0}\right)^{\alpha} \tag{1}$$

   $\eta$ is a number of particles emitted per volume per solid angle per frequency. It is a function of the distance $r$ from the central engine, of the off-axis angle $\theta$, and of the radiation frequency $\omega$.

The burst is fully specified by the following set of parameters:

- $v$, the velocity of the shell, $\gamma = \frac{1}{\sqrt{1-v^2}} \gg 1$.

  If $\gamma$ is small enough, high photon densities would make the jet plasma optically thick to pair production. This in turn would suppress emitted flux, and this is not observed. From this argument the lower bound of $\gamma \geq 100$ was derived []. The limited total energy of the burst provides an upper bound: $\gamma \leq \gamma_{\max}$ (see section 3.6). Finally, the model dependent computations of $\gamma$ give the values ranging from 50 for low-energy bursts to 1000 for high-energy ones [GNG$^+$11, GGS$^+$12]. $\gamma$ may vary from burst to burst, and it should decrease during the burst due to the dissipation of energy. As a first approximation we select $\boldsymbol{\gamma = 100}$ for this study.

- $\eta_0$, which defines the luminosity scale.

  $\eta_0$ controls the number of photons we see from the bursts, and so can be roughly estimated from the number of luminous bursts we observe. We can use this and the measured burst redshifts to estimate both $\eta_0$ and the bursts density $\rho_0$, which will be discussed later. For this study we choose $\boldsymbol{\eta_0 = 1 \times 10^{45}}$.

- $r_0$, the characteristic jet length; $r_0 \ll \frac{1}{H(0)}$, $H\left(t\right)$ is the Hubble parameter;

- $n$, which determines the sharpness of the jet end, $n > 3$;

- $\omega_0$, a characteristic radiation frequency;

- $\theta_0$, the opening angle of the jet for radiation with frequency $\omega_0$, $\theta_0 \ll 1$;

- $k$, which determines how much the opening angle changes with frequency, $k < 0$;
- $\alpha$, the bare spectral index, $\alpha < -2k - 1$

Now we have all we need to calculate the observed light curves, and then the stretching factors.

### 3.2 Photon observation time

Lets begin by computing a time at which some particular photon is observed. This time is a function of the radiator location $(r, \theta, \phi)$, as well as the observer location $(d, \chi, 0)$. (Here we choose coordinates so that the rotation angle of the observer is 0.) Lets assume for now that the observer is far enough to resolve the jet geometry, yet close enough so that the expansion of space is negligible. This assumption allows us to ignore the effects of cosmology for this calculation.

The observation time is a sum of two terms: the time interval from $t = 0$ to the photon emission (the plasma time), and the time interval between the emission and the observation (the photon time):

$$t\left(r, \theta, \phi, d, \chi\right) = t_{\text{plasma}}\left(r\right) + t_{\text{photon}}\left(r, \theta, \phi, d, \chi\right)$$

$t_{\text{plasma}}$ is easy to compute since plasma moves with uniform velocity:

$$t_{\text{plasma}}\left(r\right) = \frac{r}{v}$$

$t_{\text{photon}}$ is a distance between the radiator and the observer:

$$\begin{aligned}
t_{\text{photon}}\left(r, \theta, \phi, d, \chi\right) &= \sqrt{\left(d\cos\chi - r\cos\theta\right)^2 + \left(d\sin\chi - r\sin\theta\cos\phi\right)^2 + \left(r\sin\theta\sin\phi\right)^2} \\
&= d\sqrt{\left(\cos\chi - \frac{r}{d}\cos\theta\right)^2 + \left(\sin\chi - \frac{r}{d}\sin\theta\cos\phi\right)^2 + \left(\frac{r}{d}\sin\theta\sin\phi\right)^2} \\
&\sim d\sqrt{\cos^2\chi - 2\frac{r}{d}\cos\theta\cos\chi + \sin^2\chi - 2\frac{r}{d}\sin\theta\cos\phi\sin\chi} \\
&\sim d\left(1 - \frac{r}{d}\left(\cos\theta\cos\chi + \sin\theta\cos\phi\sin\chi\right)\right) \\
&= d - r\left(\cos\theta\cos\chi + \sin\theta\cos\phi\sin\chi\right)
\end{aligned}$$

Combining these expressions together, we get:

$$t\left(r, \theta, \phi, d, \chi\right) = d + r\left(\frac{1}{v} - \cos\theta\cos\chi - \sin\theta\cos\phi\sin\chi\right)$$

Since no photon can reach the observer faster than the speed of light, and the photons emitted at $t = 0$ reach the observer at $t = d$, this time $t = d$ is the start of the observer's light curve. So we can define a more convenient time origin:

$$\tau\left(r, \theta, \phi, \chi\right) = t\left(r, \theta, \phi, d, \chi\right) - d = r\left(\frac{1}{v} - \cos\theta\cos\chi - \sin\theta\cos\phi\sin\chi\right)$$

Finally, we can use the spherical law of cosines to write this in terms of the great-circle distance $\sigma\left(\theta, \phi, \chi\right)$ between the points $(\theta, \phi)$ and $(\chi, 0)$:

$$\tau\left(r, \theta, \phi, \chi\right) = r\left(\frac{1}{v} - \cos\sigma\left(\theta, \phi, \chi\right)\right) \tag{2}$$

Note that $\tau$ doesn't depend on $d$ anymore. But this is only true if the scale factor did not change since emission to observation. For a distant observer we should account for the change in the scale factor, which will stretch the distances between photons:

$$\tau\left(r,\theta,\phi,z,\chi\right)=r\left(\frac{1}{v}-\cos\sigma\left(\theta,\phi,\chi\right)\right)\left(1+z\right) \tag{3}$$

Here $z$ is the redshift of the burst from the point of view of the observer.

### 3.3 Cosmology

Before calculating light curves and stretching factors, we will need some equations from cosmology.

First of all, the metric of the expanding Universe:

$$\mathrm{d}s^2=-\,\mathrm{d}t^2+a^2\left(t\right)\mathrm{d}r^2+a^2\left(t\right)r^2\,\mathrm{d}\Omega_2 \tag{4}$$

We define $a\left(t_{\mathrm{obs}}\right)=1$, where $t_{\mathrm{obs}}$ is the observation time.

We need to understand how the scale factor changes with time. For that we assume that the energy content of the Universe consists of matter $\Omega_m$ and vacuum energy $\Omega_\Lambda$ only, so that the Friedmann equation takes the following form:

$$\begin{aligned}\left(\frac{\dot{a}\left(t\right)}{a\left(t\right)}\right)^2&=\Omega_m H_{\mathrm{obs}}^2\frac{1}{a^3\left(t\right)}+H_{\mathrm{obs}}^2\Omega_\Lambda\\ \dot{a}\left(t\right)&=a\left(t\right)H_{\mathrm{obs}}\sqrt{\Omega_m\frac{1}{a^3\left(t\right)}+\Omega_\Lambda}\\ \mathrm{d}t&=\frac{\mathrm{d}a}{a\left(t\right)H_{\mathrm{obs}}\sqrt{\Omega_m\frac{1}{a^3(t)}+\Omega_\Lambda}}\end{aligned}$$

Here $H_{\mathrm{obs}}=H\left(t_{\mathrm{obs}}\right)=\dot{a}\left(t_{\mathrm{obs}}\right)$ is the Hubble parameter at the observation time.

We also need to know the areas of two spheres: the photon sphere, a sphere over which photons emitted in a particular burst are spread; and the bursts sphere, a sphere over which bursts at a particular redshift are distributed.

Lets begin with the photon sphere. This sphere has the origin at $r=0$ and $t=0$, at the central engine of a particular burst. Taking $\mathrm{d}s=0$ and $\mathrm{d}\Omega_2=0$ in the equation for metric, we get:

$$\mathrm{d}r=\frac{\mathrm{d}t}{a\left(t\right)}$$

And now we integrate over time to find the observer's position:

$$\begin{aligned}r\left(t_{\mathrm{obs}}\right)&=\int_0^{t_{\mathrm{obs}}}\frac{\mathrm{d}t}{a\left(t\right)}\\ &=\int_{a(0)}^{1}\frac{\mathrm{d}a}{a^2\left(t\right)H_{\mathrm{obs}}\sqrt{\Omega_m\frac{1}{a^3(t)}+\Omega_\Lambda}}\\ &=\frac{{}_2F_1\left(\frac{1}{3},\frac{1}{2};\frac{4}{3};-\frac{\Omega_m}{a^3(0)\Omega_\Lambda}\right)-a\left(0\right){}_2F_1\left(\frac{1}{3},\frac{1}{2};\frac{4}{3};-\frac{\Omega_m}{\Omega_\Lambda}\right)}{a\left(0\right)H_{\mathrm{obs}}\sqrt{\Omega_\Lambda}}\end{aligned}$$

Here ${}_2F_1\left(a,b;c;z\right)=\frac{\Gamma(c)}{\Gamma(b)\Gamma(c-b)}\int_0^1\frac{t^{b-1}(1-t)^{c-b-1}}{(1-tz)^a}\,\mathrm{d}t$ is a hypergeometric function. Here $a\left(0\right)=\frac{1}{1+z}$, so, finally,

$$r\left(z\right)=\frac{\left(1+z\right){}_2F_1\left(\frac{1}{3},\frac{1}{2};\frac{4}{3};-\frac{\Omega_m}{\Omega_\Lambda}\left(1+z\right)^3\right)-{}_2F_1\left(\frac{1}{3},\frac{1}{2};\frac{4}{3};-\frac{\Omega_m}{\Omega_\Lambda}\right)}{H_{\mathrm{obs}}\sqrt{\Omega_\Lambda}} \tag{5}$$

The area of the photon sphere is then:

$$A_{\mathrm{ph}}(z) = 4\pi a^2(t_{\mathrm{obs}})\, r^2(z) = 4\pi r^2(z) \tag{6}$$

The second sphere is the bursts sphere. It has its origin at the observer's position. We define a new primed set of coordinates, so that $r' = 0$ and $t' = 0$ at the observation event. We can relate the primed coordinates of the burst to the observer's unprimed coordinates:

$$\begin{aligned} t'_{\mathrm{burst}} &= -t_{\mathrm{obs}} \\ r'\left(t'_{\mathrm{burst}}\right) = r'\left(-t_{\mathrm{obs}}\right) &= \int_{-t_{\mathrm{obs}}}^{0} \frac{\mathrm{d}t'}{a'(t')} = \int_{0}^{t_{\mathrm{obs}}} \frac{\mathrm{d}t}{a(t)} = r(t_{\mathrm{obs}}) \end{aligned}$$

We see that the radius of the bursts sphere is the same as the radius of the photon sphere. Finally, the area is:

$$A_{\mathrm{b}}(z) = 4\pi a'^2(-t_{\mathrm{obs}})\, r^2(z) = 4\pi a^2(0)\, r^2(z) = \frac{4\pi r^2(z)}{(1+z)^2} \tag{7}$$

We will need to know one more thing about the bursts sphere – the volume of the infinitesimal shell surrounding it. For that we can again use the metric:

$$\begin{aligned} \mathrm{d}V(z) &= -A_{\mathrm{b}}(z)\, a(0)\, \mathrm{d}r \\ &= -A_{\mathrm{b}}(z)\, a(0) \frac{\mathrm{d}a}{a^2(0)\, H_{\mathrm{obs}} \sqrt{\Omega_m \frac{1}{a^3(t)} + \Omega_\Lambda}} \\ &= A_{\mathrm{b}}(z) \frac{\frac{1}{(1+z)^2}\, \mathrm{d}z\, (1+z)}{H_{\mathrm{obs}} \sqrt{\Omega_m \frac{1}{a^3(t)} + \Omega_\Lambda}} \\ &= A_{\mathrm{b}}(z) \frac{1}{(1+z)} \frac{\mathrm{d}z}{H_{\mathrm{obs}} \sqrt{\Omega_m (1+z)^3 + \Omega_\Lambda}} \\ &= \frac{4\pi r^2(z)}{(1+z)^3} \frac{\mathrm{d}z}{H_{\mathrm{obs}} \sqrt{\Omega_m (1+z)^3 + \Omega_\Lambda}} \end{aligned} \tag{8}$$

### 3.4 Light curve

We now know enough to compute the observable quantity - the number of observed photons $p$. For that we need to integrate the radiation intensity $\eta$ over four things. Two burst-related things: radiator positions and frequencies at emission. Two observer-related things: observation time and frequencies at observation. We relate the first two and the second two with the delta functions:

$$\begin{aligned} p(z, \chi; \tau_1, \tau_2; \omega_1, \omega_2) = \frac{A_{\mathrm{det}}}{A_{\mathrm{ph}}(z)} \int_0^\infty \mathrm{d}r \int_0^\pi r\, \mathrm{d}\theta \int_0^{2\pi} r \sin\theta\, \mathrm{d}\phi \int_0^\infty \mathrm{d}\omega' \int_{\tau_1}^{\tau_2} \mathrm{d}\tau \int_{\omega_1}^{\omega_2} \mathrm{d}\omega\, \eta\left(r, \theta, \omega'\right) \\ \times \underbrace{\frac{1}{\gamma^2\left(1 - v\cos\sigma(\theta, \phi, \chi)\right)^2}}_{\text{aberration}} \underbrace{\frac{1}{\gamma\left(1 - v\cos\sigma(\theta, \phi, \chi)\right)}}_{\text{time dilation}} \\ \times \delta\left( \underbrace{\frac{\omega'}{\gamma\left(1 - v\cos\sigma(\theta, \phi, \chi)\right)}}_{\text{relativistic shift}} \underbrace{(1+z)}_{\text{cosmological shift}} - \omega \right) \end{aligned}$$

$$\times \delta\left(\tau - r\left(\frac{1}{v} - \cos\sigma\left(\theta,\phi,\chi\right)\right)(1+z)\right) \tag{9}$$

Here $A_{\rm det}$ is the effective area of the detector. We have taken account for the four relativistic effects, which affect intensities and frequencies of the radiators: relativistic aberration; time dilation of the radiators relative to the observer; relativistic blue/redshift; and cosmological redshift.

We can use the delta functions to do the integrals over $\omega'$ and $r$. For that lets transform the first one:

$$\begin{aligned}\delta\left(\frac{\omega'}{\gamma\left(1-v\cos\sigma\right)(1+z)} - \omega\right) &= \delta\left(\frac{1}{\gamma\left(1-v\cos\sigma\right)(1+z)}\left(\omega' - \gamma\left(1-v\cos\sigma\right)(1+z)\,\omega\right)\right)\\ &= \gamma\left(1-v\cos\sigma\right)(1+z)\,\delta\left(\omega' - \gamma\left(1-v\cos\sigma\right)(1+z)\,\omega\right)\end{aligned}$$

And the second one:

$$\begin{aligned}\delta\left(\tau - r\left(\frac{1}{v} - \cos\sigma\right)(1+z)\right) &= \delta\left(\left(\frac{1}{v} - \cos\sigma\right)(1+z)\left(r - \frac{\tau}{\left(\frac{1}{v} - \cos\sigma\right)(1+z)}\right)\right)\\ &= \frac{1}{\left(\frac{1}{v} - \cos\sigma\right)(1+z)}\delta\left(r - \frac{\tau}{\left(\frac{1}{v} - \cos\sigma\right)(1+z)}\right)\end{aligned}$$

After the transformations the expression for $p$ takes the following form:

$$\begin{aligned}p\left(z,\chi;\tau_1,\tau_2;\omega_1,\omega_2\right) = \frac{A_{\rm det}}{A_{\rm ph}\left(z\right)}&\int_0^{\pi}\mathrm{d}\theta\int_0^{2\pi}\mathrm{d}\phi\int_{\tau_1}^{\tau_2}\mathrm{d}\tau\int_{\omega_1}^{\omega_2}\mathrm{d}\omega\\ &\times\eta\left(\frac{\tau}{\left(\frac{1}{v}-\cos\sigma\left(\theta,\phi,\chi\right)\right)(1+z)},\theta,\gamma\left(1-v\cos\sigma\left(\theta,\phi,\chi\right)\right)(1+z)\,\omega\right)\\ &\times\frac{\tau^2\sin\theta}{\left(\frac{1}{v}-\cos\sigma\left(\theta,\phi,\chi\right)\right)^3(1+z)^2\gamma^2\left(1-v\cos\sigma\left(\theta,\phi,\chi\right)\right)^2}\\ =\frac{A_{\rm det}}{A_{\rm ph}\left(z\right)}\frac{1}{v^2\gamma^2(1+z)^2}&\int_{\tau_1}^{\tau_2}\mathrm{d}\tau\,\tau^2\int_0^{\frac{\pi}{2}}\mathrm{d}\theta\int_0^{2\pi}\mathrm{d}\phi\int_{\omega_1}^{\omega_2}\mathrm{d}\omega\frac{\sin\theta}{\left(\frac{1}{v}-\cos\sigma\left(\theta,\phi,\chi\right)\right)^5}\\ &\times\eta\left(\frac{\tau}{\left(\frac{1}{v}-\cos\sigma\left(\theta,\phi,\chi\right)\right)(1+z)},\theta,\gamma\left(1-v\cos\sigma\left(\theta,\phi,\chi\right)\right)(1+z)\,\omega\right)\end{aligned} \tag{10}$$

Furthermore, we can do the integrals over $\omega$ and $\tau$, if we write $\eta$ explicitly:

$$\begin{aligned}p\left(z,\chi;\tau_1,\tau_2;\omega_1,\omega_2\right) = \frac{A_{\rm det}}{A_{\rm ph}\left(z\right)}\frac{1}{v^2\gamma^2(1+z)^2}&\int_0^{\pi}\mathrm{d}\theta\int_0^{2\pi}\mathrm{d}\phi\int_{\omega_1}^{\omega_2}\mathrm{d}\omega\int_{\tau_1}^{\tau_2}\mathrm{d}\tau\,\tau^2\frac{\sin\theta}{\left(\frac{1}{v}-\cos\sigma\left(\theta,\phi,\chi\right)\right)^5}\\ &\times\frac{\eta_0}{1+\left(\frac{\tau}{r_0\left(\frac{1}{v}-\cos\sigma(\theta,\phi,\chi)\right)(1+z)}\right)^n}\\ &\times\exp\left(-\left(\frac{\theta}{\theta_0}\right)^2\left(\frac{\omega\gamma\left(1-v\cos\sigma\left(\theta,\phi,\chi\right)\right)(1+z)}{\omega_0}\right)^{-2k}\right)\\ &\times\left(\frac{\omega\gamma\left(1-v\cos\sigma\left(\theta,\phi,\chi\right)\right)(1+z)}{\omega_0}\right)^{\alpha}\\ =\frac{A_{\rm det}}{A_{\rm ph}\left(z\right)}\frac{\eta_0}{\left(v\gamma\left(1+z\right)\right)^{2-\alpha}}&\int_0^{\pi}\mathrm{d}\theta\int_0^{2\pi}\mathrm{d}\phi\frac{\sin\theta}{\left(\frac{1}{v}-\cos\sigma\left(\theta,\phi,\chi\right)\right)^{5-\alpha}}\end{aligned}$$

$$\times \int_{\omega_1}^{\omega_2} \mathrm{d}\omega \exp\left(-\left(\frac{\theta}{\theta_0}\right)^2 \left(\frac{\omega\gamma\left(1 - v\cos\sigma\left(\theta,\phi,\chi\right)\right)(1+z)}{\omega_0}\right)^{-2k}\right)\left(\frac{\omega}{\omega_0}\right)^{\alpha}$$
$$\times \int_{\tau_1}^{\tau_2} \mathrm{d}\tau\, \tau^2 \frac{1}{1+\left(\frac{\tau}{r_0\left(\frac{1}{v}-\cos\sigma(\theta,\phi,\chi)\right)(1+z)}\right)^n}$$
$$= \frac{A_{\mathrm{det}}}{A_{\mathrm{ph}}\left(z\right)} \frac{\eta_0}{\left(v\gamma\left(1+z\right)\right)^{2-\alpha}} \int_0^{\pi} \mathrm{d}\theta \int_0^{2\pi} \mathrm{d}\phi \frac{\sin\theta}{\left(\frac{1}{v} - \cos\sigma\left(\theta,\phi,\chi\right)\right)^{5-\alpha}}$$
$$\times \left(I\left(z,\chi,\omega_2;\theta,\phi\right) - I\left(z,\chi,\omega_1;\theta,\phi\right)\right)\left(J\left(z,\chi,\tau_2;\theta,\phi\right) - J\left(z,\chi,\tau_1;\theta,\phi\right)\right) \quad (11)$$

Here $I$ and $J$ are the indefinite integrals over $\omega$ and $\tau$:

$$I\left(z,\chi,\omega;\theta,\phi\right) = \frac{\omega\left(\frac{\omega}{\omega_0}\right)^{\alpha} E_{\frac{\alpha+1}{2k}+1}\left(\left(\frac{\theta}{\theta_0}\right)^2\left(\frac{\omega}{\omega_0}\right)^{-2k}\left(\gamma\left(1 - v\cos\sigma\left(\theta,\phi,\chi\right)\right)(1+z)\right)^{-2k}\right)}{2k} \quad (12)$$

$$J\left(z,\chi,\tau;\theta,\phi\right) = \frac{\tau^3}{3}\,{}_2F_1\left(1,\frac{3}{n};\frac{n+3}{n};-\left(\frac{\tau}{r_0\left(\frac{1}{v}-\cos\sigma\left(\theta,\phi,\chi\right)\right)(1+z)}\right)^n\right) \quad (13)$$

where $E_n$ function $E_n\left(x\right) = \int_1^{\infty} \frac{e^{-xt}\,\mathrm{d}t}{t^n}$.

The remaining integrals over $\theta$ and $\chi$ are hard to do symbolically, so we compute them numerically. To optimize this computation we can use the assumption of small $\theta$ and $\chi$, so that:

$$\sin\theta \sim \theta$$
$$\cos\sigma\left(\theta,\phi,\chi\right) = \cos\theta\cos\chi + \sin\theta\sin\chi\cos\phi \sim 1 - \frac{\theta^2}{2} - \frac{\chi^2}{2} + \theta\chi\cos\phi$$

Using that, and the observation that this integral is an even function of $\theta$, we arrive to the optimized expressions for $p$, $I$ and $J$:

$$p\left(z,\chi;\tau_1,\tau_2;\omega_1,\omega_2\right) = \frac{A_{\mathrm{det}}}{A_{\mathrm{ph}}\left(z\right)} \frac{2\eta_0}{\left(v\gamma\left(1+z\right)\right)^{2-\alpha}} \int_0^{\infty} \mathrm{d}\theta \int_0^{\pi} \mathrm{d}\phi \frac{\theta}{\left(\frac{1}{v} - 1 + \frac{\theta^2}{2} + \frac{\chi^2}{2} - \theta\chi\cos\phi\right)^{5-\alpha}}$$
$$\times \left(I\left(z,\chi,\omega_2;\theta,\phi\right) - I\left(z,\chi,\omega_1;\theta,\phi\right)\right)\left(J\left(z,\chi,\tau_2;\theta,\phi\right) - J\left(z,\chi,\tau_1;\theta,\phi\right)\right) \quad (14)$$

$$I\left(z,\chi,\omega;\theta,\phi\right) = \frac{\omega\left(\frac{\omega}{\omega_0}\right)^{\alpha} E_{\frac{\alpha+1}{2k}+1}\left(\left(\frac{\theta}{\theta_0}\right)^2\left(\frac{\omega}{\omega_0}\right)^{-2k}\left(v\gamma\left(1+z\right)\left(\frac{1}{v} - 1 + \frac{\theta^2}{2} + \frac{\chi^2}{2} - \theta\chi\cos\phi\right)\right)^{-2k}\right)}{2k} \quad (15)$$

$$J\left(z,\chi,\tau;\theta,\phi\right) = \frac{\tau^3}{3}\,{}_2F_1\left(1,\frac{3}{n};\frac{n+3}{n};-\left(\frac{\tau}{r_0\left(\frac{1}{v} - 1 + \frac{\theta^2}{2} + \frac{\chi^2}{2} - \theta\chi\cos\phi\right)(1+z)}\right)^n\right) \quad (16)$$

Finally, we will need to compute limits of $p$ for $\omega_2 \to \infty$ and $\tau_2 \to \infty$. It requires us to know the limit of $I$ for $\omega \to \infty$ (we assumed that $k < 0$):

$$I\left(z,\chi,\infty;\theta,\phi\right) = \lim_{\omega\to\infty} I\left(z,\chi,\omega;\theta,\phi\right) = 0 \quad (17)$$

and the limit of $J$ for $\tau \to \infty$ ($n > 3$ by assumption):

$$J\left(z,\chi,\infty;\theta,\phi\right) = \lim_{\tau\to\infty} J\left(z,\chi,\tau;\theta,\phi\right) = \left(r_0\left(\frac{1}{v} - 1 + \frac{\theta^2}{2} + \frac{\chi^2}{2} - \theta\chi\cos\phi\right)(1+z)\right)^3 \frac{\pi}{n\sin\frac{3\pi}{n}} \quad (18)$$

Now, when we know $p$, we can compute many different things with it. Examples include:

- the total number of particles observed in a given energy range, $p_\infty(z,\chi;\omega_1,\omega_2) = p(z,\chi;0,\infty;\omega_1,\omega_2)$;
- the fraction of photons observed during a given time interval, $\Phi(z,\chi;\tau_1,\tau_2;\omega_1,\omega_2) = \frac{p(z,\chi;\tau_1,\tau_2;\omega_1,\omega_2)}{p_\infty(z,\chi;\omega_1,\omega_2)}$;
- the duration of the burst $T_f(z,\chi;\omega_1,\omega_2)$, that is the time by which the fraction $f$ of photons is observed. We can compute it by solving the following equation for $T_f$: $p\left(z,\chi;0,T_f;\omega_1,\omega_2\right) = f p_\infty(z,\chi;\omega_1,\omega_2)$;
- the stretching factor, which we will discuss in the next section.

### 3.5 Stretching factor

The stretching factor for a continuous light curve is defined exactly like the stretching factor for a discrete one. It is the value of $\kappa$ which makes the KS-distance minimal:

$$\kappa(z,\chi;\omega_1,\omega_2,\omega_3) = \operatorname*{argmin}_\kappa \max_\tau \left|\Phi(z,\chi;0,\tau;\omega_1,\omega_2) - \Phi(z,\chi;0,\kappa\tau;\omega_2,\omega_3)\right| \tag{19}$$

The maximum of an absolute value cannot be differentiated, so the computation of $\kappa$ by the given definition is complicated. Lets instead rewrite this expression in terms of a positive and a negative KS-distances:

$$\begin{aligned}
D_+(z,\chi;\kappa;\omega_1,\omega_2,\omega_3) &= \max_\tau \left(\Phi(z,\chi;0,\tau;\omega_1,\omega_2) - \Phi(z,\chi;0,\kappa\tau;\omega_2,\omega_3)\right)\\
D_-(z,\chi;\kappa;\omega_1,\omega_2,\omega_3) &= \min_\tau \left(\Phi(z,\chi;0,\tau;\omega_1,\omega_2) - \Phi(z,\chi;0,\kappa\tau;\omega_2,\omega_3)\right)\\
\kappa(z,\chi;\omega_1,\omega_2,\omega_3) &= \operatorname*{argmin}_\kappa \max\left(D_+(z,\chi;\kappa;\omega_1,\omega_2,\omega_3), -D_-(z,\chi;\kappa;\omega_1,\omega_2,\omega_3)\right)
\end{aligned}$$

Take note that $\Phi$ monotonously increases with $\tau$. It implies that $D_+$ and $D_-$ monotonously decrease with $\kappa$, so as $D_+ + D_-$. So there is a single value of $\kappa$, for which

$$D_+(z,\chi;\kappa;\omega_1,\omega_2,\omega_3) = -D_-(z,\chi;\kappa;\omega_1,\omega_2,\omega_3) \tag{20}$$

And this value of $\kappa$ also makes the $\max(D_+,-D_-)$ minimal, since $D_+$ monotonously decrease, and $-D_-$ monotonously increase with $\kappa$.

So we have now a simpler way to compute $\kappa$ by solving an equation instead of computing the minimum. And $\Phi$ can be differentiated, which makes it easier to compute maximums and minimums of their differences.

Being able to compute the stretching factor, we could now compare our model predictions with observations given the position of an observer. We don't know the observer's off-axis angle $\chi$, however, so we cannot check the stretching factor prediction directly. Instead, we will focus on a series of tests, which will ensure that our model doesn't contradict existing observations. These tests will be discussed in the following sections.

### 3.6 Total energy

The first test is to compute the total energy radiated from the burst, and to ensure that it doesn't exceed the mass of the star from which the burst originated.

To compute the total energy, we need to multiply the radiation intensity by frequency, and integrate it over frequencies $\omega$, volume $(r,\theta,\phi)$, and observer positions $(\sigma,\xi)$. We assumed $\theta \ll 1$, and have taken into account the same relativistic effects as we did in the observed particle count computation:

$$E = \int_0^\infty \mathrm{d}\omega \int_0^\infty \mathrm{d}r \int_0^\infty r\,\mathrm{d}\theta \int_0^{2\pi} r\,\theta\,\mathrm{d}\phi \int_0^\infty \mathrm{d}\sigma \int_0^{2\pi} \sin\sigma\,\mathrm{d}\xi$$

$$\times \eta(r,\theta,\omega)\underbrace{\frac{1}{\gamma(1-v\cos\sigma)}}_{\text{time dilation}}\underbrace{\frac{1}{\gamma^2(1-v\cos\sigma)^2}}_{\text{aberration}}\underbrace{\frac{\omega}{\gamma(1-v\cos\sigma)}}_{\text{relativistic shift}} \tag{21}$$

$$= \frac{4\pi^2}{\gamma^4}\int_0^\infty \mathrm{d}\omega\,\omega\int_0^\infty \mathrm{d}r\,r^2\int_0^\infty \mathrm{d}\theta\,\theta\,\eta(r,\theta,\omega)\int_0^\infty \mathrm{d}\sigma\frac{\sin\sigma}{(1-v\cos\sigma)^4}$$

An integral over $\sigma$ is computable analytically:

$$\int_0^\infty \mathrm{d}\sigma\frac{\sin\sigma}{(1-v\cos\sigma)^4} = \frac{2\left(3+v^2\right)}{3\left(1-v^2\right)^3} = \frac{2}{3}\gamma^6\left(4-\frac{1}{\gamma^2}\right)$$

Substituting this result into the expression for $E$ we get:

$$E = \frac{32\pi^2}{3}\left(\gamma^2-\frac{1}{4}\right)\int_0^\infty \mathrm{d}\omega\,\omega\int_0^\infty \mathrm{d}r\,r^2\int_0^\infty \mathrm{d}\theta\,\theta\,\eta(r,\theta,\omega) \tag{22}$$

Now we can use the expression for $\eta$ to do the remaining integrals:

$$E = \frac{32\pi^2\eta_0}{3}\left(\gamma^2-\frac{1}{4}\right)\int_0^\infty \mathrm{d}\omega\,\omega\left(\frac{\omega}{\omega_0}\right)^\alpha\int_0^\infty \mathrm{d}r\,\frac{r^2}{1+\left(\frac{r}{r_0}\right)^n}\int_0^\infty \mathrm{d}\theta\,\theta\,\exp\left(-\left(\frac{\theta}{\theta_0}\right)^2\left(\frac{\omega}{\omega_0}\right)^{-2k}\right)$$

The integrals over $r$ and $\theta$ can be done symbolically:

$$\int_0^\infty \mathrm{d}r\,\frac{r^2}{1+\left(\frac{r}{r_0}\right)^n} = \frac{\pi}{n\sin\left(\frac{3\pi}{n}\right)}r_0^3$$

$$\int_0^\infty \mathrm{d}\theta\,\theta\,\exp\left(-\left(\frac{\theta}{\theta_0}\right)^2\left(\frac{\omega}{\omega_0}\right)^{-2k}\right) = \frac{1}{2}\theta_0^2\left(\frac{\omega}{\omega_0}\right)^{2k}$$

Now we only have one integral left:

$$E = \frac{16\pi^3}{3n\sin\left(\frac{3\pi}{n}\right)}\left(\gamma^2-\frac{1}{4}\right)\eta_0\,r_0^3\,\theta_0^2\int_0^\infty \mathrm{d}\omega\,\omega\left(\frac{\omega}{\omega_0}\right)^{2k+\alpha} \tag{23}$$

Note, however, that since $\alpha < -2k-1$ this integral diverges for $\omega \to 0$. But our model is not expected to describe low-energy radiation of the burst, so we should not integrate over low-frequency radiators. Nevertheless, we should ensure that the total energy of the high-energy radiation is not too large. To compute this energy we will only integrate over those radiators which emission we can observe, that is over the radiators with frequencies greater than $\frac{\omega_1}{\gamma}$, where $\omega_1$ is the smallest observable photon frequency. Now we can compute the last integral and get the final expression for $E$:

$$\begin{aligned}
E(\omega_1) &= \frac{16\pi^3}{3n\sin\left(\frac{3\pi}{n}\right)}\left(\gamma^2-\frac{1}{4}\right)\eta_0\,r_0^3\,\theta_0^2\int_{\frac{\omega_1}{\gamma}}^\infty \mathrm{d}\omega\,\omega\left(\frac{\omega}{\omega_0}\right)^{2k+\alpha} \\
&= \frac{16\pi^3}{3n\sin\left(\frac{3\pi}{n}\right)}\left(\gamma^2-\frac{1}{4}\right)\eta_0\,r_0^3\,\theta_0^2\frac{\omega_1^2\left(\frac{\omega_1}{\gamma\omega_0}\right)^{2k+\alpha}}{\gamma^2(-2k-\alpha-2)} \\
&= \frac{16\pi^3}{3n\left(-2k-\alpha-2\right)\sin\left(\frac{3\pi}{n}\right)}\gamma^{-2k-\alpha}\left(1-\frac{1}{4\gamma^2}\right)\eta_0\,r_0^3\,\theta_0^2\frac{\omega_0^{-2k-\alpha}}{\omega_1^{-2k-\alpha-2}}
\end{aligned} \tag{24}$$

This energy should not be larger than a typical mass $M_s$ of a massive star. So, finally, we arrive at the first constraint for the burst parameters:

$$\frac{16\pi^3}{3n\left(-2k-\alpha-2\right)\sin\left(\frac{3\pi}{n}\right)}\gamma^{-2k-\alpha}\left(1-\frac{1}{4\gamma^2}\right)\eta_0\,r_0^3\,\theta_0^2\frac{\omega_0^{-2k-\alpha}}{\omega_1^{-2k-\alpha-2}} < M_s \tag{25}$$

### 3.7 Distribution of stretching factors

The second test is to calculate the distribution of the stretching factors of the observable bursts, and to compare it with observations.

The computation of the exact and precise distribution is technically hard (because stretching factors neither change monotonously with redshift, nor with off-axis angle), and computationally intensive. So we will not compute the precise distribution.

Instead, we will use the Monte-Carlo method to produce a large representative sample of stretching factors. Then, we will calculate an empirical CDF of this sample, which can be compared with observations using the KS-test. Since we can compute much larger sample than that of observations, we will not lose much precision due to this simplification.

We still have one ingredient missing though – the evolution of the bursts density. We assume that the density is roughly proportional to the stars density, and the stars density is roughly proportional to the matter density, which changes with $z$ as $(1+z)^3$. It is clear, however, that since no stars existed at very small redshifts, the burst density should decline there, so we add an exponential cutoff to it:

$$\rho = \rho_0 (1+z)^3 \exp\left(-\frac{z}{z_c}\right) \tag{26}$$

Here $\rho_0$ is a normalization factor, and $z_c$ is a redshift scale, after which the density is cut off.

Now when we have all the ingredients, we can compute the sample with the following steps:

1. First of all we need to define the range from which to select redshifts and off-axis angles. We should include all observable jet positions in this range. However, to avoid dropping too many points corresponding to invisible bursts, we should keep the range as small as possible. We also want to make the region rectangular to be able to select redshifts and angles separately.

   Lets start by selecting a range for redshifts. Ideally, we want this range to start with $z = 0$. Then, however, there will be visible jets for all possible off-axis angles, which will make our angles range too large. Note also, that since the bursts count increases with redshift as $z^3$, the probability to observe a low-redshift burst is very small. So instead of selecting the smallest redshift to be 0, we select it to be a small number $z_{\min}$.

   $z_{\max}$ is defined by the farthest jet, which can be observed. Since the burst observability $p_\infty(z, \chi, \omega_2, \omega_3)$ decreases with both redshift and $\chi$, we can find the maximum redshift by solving the following equation:

   $$p_\infty(z_{\max}, 0, \omega_2, \omega_3) = p_{\min} \tag{27}$$

   where $p_{\min}$ is the minimum number of particles required to claim an observation.

2. The range for off-axis angles is easier to compute since nothing prohibits us from selecting the smallest angle to be 0.

   The observability declines with $z$ and $\chi$, so the observable burst with the largest $\chi$ should be located at the redshift $z_{\min}$. We can find this angle by solving the similar equation, as we did for the redshifts:

   $$p_\infty(z_{\min}, \chi_{\max}, \omega_2, \omega_3) = p_{\min} \tag{28}$$

3. Now we are in a position to select a particular properly distributed random redshift. The CDF of the distribution of redshifts is a ratio of redshift counts in different space volumes:

   $$\Phi_z(z) = \frac{\int_{z_{\min}}^{z} \rho(z')\,\mathrm{d}V(z')}{\int_{z_{\max}}^{z_{\max}} \rho(z')\,\mathrm{d}V(z')} \tag{29}$$

   To generate a redshift, we should uniformly select a value of $\Phi_z$, and solve the corresponding equation for $z$:

   $$\Phi_z(z) = x \tag{30}$$

   where $x$ is a random variable uniformly distributed in the range 0 to 1.

4. An off-axis angle can be selected in a similar way. The CDF of the angles distribution is a ratio of spherical areas:

$$\Phi_\chi(\chi) = \frac{\int_0^\chi \sin\chi' \,\mathrm{d}\chi'}{\int_0^{\chi_{\max}} \sin\chi' \,\mathrm{d}\chi'} \approx \frac{\int_0^\chi \chi' \,\mathrm{d}\chi'}{\int_0^{\chi_{\max}} \chi' \,\mathrm{d}\chi'} = \left(\frac{\chi}{\chi_{\max}}\right)^2 \tag{31}$$

As with redshifts, we get a properly distributed $\chi$ by solving the equation:

$$\Phi_\chi(\chi) = \left(\frac{\chi}{\chi_{\max}}\right)^2 = y \tag{32}$$

$$\chi = \chi_{\max}\sqrt{y} \tag{33}$$

Here $y$ is an another random variable uniformly distributed in the range 0 to 1.

5. Now we should check, if the burst in a selected position can be observed: $p_\infty(z, \chi, \omega_2, \omega_3) > p_{\min}$. If it is, add $\kappa(z, \chi)$ to the sample. If not, repeat from the step 3.

6. If the sample is not as big as we want yet, repeat from the step 3.

Our set of parameters led to a sample you can see on the figure 3. However, the error margins of the observed stretching factors are too large to use the KS-test on them. Nevertheless, it appears that our model doesn't contradict existing observations.

### 3.8 Very high energy bursts fraction

Out final test is the comparison of answers to this question: given the bursts which were observed in a high energy range $(\omega_1, \omega_3)$, which fraction of them can also be observed in a very high energy range $(\omega_2, \omega_3)$?

To calculate this value, we need to compute the number of bursts visible in a given energy range, which is the integral over space and jet directions:

$$\begin{aligned} b(\omega_1, \omega_2) &= \int_0^{z_{\max}(\omega_1,\omega_2)} \mathrm{d}V(z)\,\rho(z) \int_0^{\chi_{\max}(z,\omega_1,\omega_2)} 2\pi \sin\chi \,\mathrm{d}\chi \\ &\approx 2\pi \int_0^{z_{\max}(\omega_1,\omega_2)} \mathrm{d}V(z)\,\rho(z) \int_0^{\chi_{\max}(z,\omega_1,\omega_2)} \chi \,\mathrm{d}\chi = \pi \int_0^{z_{\max}(\omega_1,\omega_2)} \mathrm{d}V(z)\,\rho(z)\,\chi^2_{\max}(z, \omega_1, \omega_2) \end{aligned} \tag{34}$$

Here $z_{\max}(\omega_1, \omega_2)$ and $\chi_{\max}(z, \omega_1, \omega_2)$ are the same values we used in the previous section: the maximum redshift from which a burst can be observed in a given energy range, and the maximum off-axis angle with which the burst at redshift $z$ can be observed.

The fraction we want to compute is the ratio of these integrals:

$$f(\omega_1, \omega_2, \omega_3) = \frac{b(\omega_2, \omega_3)}{b(\omega_1, \omega_3)} = \frac{\int_0^{z_{\max}(\omega_2,\omega_3)} \mathrm{d}V(z)\,\rho(z)\,\chi^2_{\max}(z, \omega_2, \omega_3)}{\int_0^{z_{\max}(\omega_1,\omega_3)} \mathrm{d}V(z)\,\rho(z)\,\chi^2_{\max}(z, \omega_1, \omega_3)} \tag{35}$$

The ratio for our set of parameters is $f_m = 0.072$. The LAT burst catalog [AAA+13] contains $n = 35$ bursts, 3 of which were observed in the energy range $(1\,\mathrm{GeV}, \infty)$. So the ratio is $f_o = \frac{3}{35} \approx 0.086$. The binary distribution gives us the probability for it to happen:

$$\Pr\left(f_o = \frac{k}{n}\right) = \binom{n}{k} f_m^k (1 - f_m)^{n-k} \approx 0.22 \tag{36}$$

which means that the model doesn't contradict observations in this test.

### 3.9 Parameter values

### 3.10 Results

## 4 Discussion

## References


[AAA+13] M. Ackermann, M. Ajello, K. Asano, M. Axelsson, L. Baldini et al., *The First Fermi-LAT Gamma-Ray Burst Catalog*, Astrophys.J.Suppl. **209**, 11 (2013), 1303.2908.

[BFK03] J. S. Bloom, D. Frail and S. Kulkarni, *GRB energetics and the GRB Hubble diagram: Promises and limitations*, Astrophys.J. **594**, 674–683 (2003), astro-ph/0302210.

[Fermi-LAT12] M. Ackermann et al. (Fermi-LAT Collaboration), *The Fermi Large Area Telescope On Orbit: Event Classification, Instrument Response Functions, and Calibration*, Astrophys.J.Suppl. **203**, 4 (2012), 1206.1896.

[Fermi11] M. Ackermann et al. (Fermi Collaboration), *Detection of a spectral break in the extra hard component of GRB 090926A*, Astrophys.J. **729**, 114 (2011), 1101.2082.

[FLG09] H. Tajima (Fermi-LAT and GBM Collaborations), *Fermi Observations of high-energy gamma-ray emissions from GRB 080916C*, (2009), 0907.0714.

[FS09] A. Abdo et al. (Fermi/GBM, Fermi/LAT and Swift Collaborations), *Fermi Observations of GRB 090902B: A Distinct Spectral Component in the Prompt and Delayed Emission*, Astrophys.J. **706**, L138–L144 (2009), 0909.2470.

[GGS+12] G. Ghisellini, G. Ghirlanda, R. Salvaterra, L. Nava, D. Burlon et al., *GRBs have preferred jet opening angles and bulk Lorentz factors*, (2012), 1211.2062.

[GNG+11] G. Ghirlanda, L. Nava, G. Ghisellini, A. Celotti, D. Burlon et al., *Gamma Ray Bursts in the comoving frame*, (2011), 1107.4096.

[GR13] N. Gehrels and S. Razzaque, *Gamma Ray Bursts in the Swift-Fermi Era*, Front.Phys.China. **8**, 661–678 (2013), 1301.0840.

[LP13] J. Lange and M. Pohl, *The average GeV-band Emission from Gamma-Ray Bursts*, (2013), 1301.2914.

[NI01] T. Nakamura and K. Ioka, *Peak luminosity-spectral lag relation caused by the viewing angle of the collimated gamma-ray bursts*, (2001), astro-ph/0105321.

[RPT12] G. Rubtsov, M. Pshirkov and P. Tinyakov, *GRB observations by Fermi LAT revisited: new candidates found*, Mon.Not.Roy.Astron.Soc.Lett. **421**, L14–L18 (2012), 1104.5476.

[Science04] N. Gehrels et al. (Swift Science Collaboration), *The Swift Gamma-Ray Burst Mission*, AIP Conf.Proc. **727**, 637–641 (2004), astro-ph/0405233.

[SSD+13] A. Shenoy, E. Sonbas, C. Dermer, L. Maximon, K. Dhuga et al., *Probing Curvature Effects in the Fermi GRB 110920*, Astrophys.J. **778**, 3 (2013), 1304.4168.

[SSL05] R.-F. Shen, L.-M. Song and Z. Li, *Spectral lags and the energy dependence of pulse width in gamma-ray bursts: Contributions from the relativistic curvature effect*, Mon.Not.Roy.Astron.Soc. **362**, 59–65 (2005), astro-ph/0505276.

[Via13] G. Vianello, *Observations of Gamma-ray Bursts in the Fermi era*, (2013), 1304.5570.

[YLQL06] T.-F. Yi, E.-W. Liang, Y.-P. Qin and R.-J. Lu, *On the spectral lags of the short gamma-ray bursts*, Mon.Not.Roy.Astron.Soc. **367**, 1751–1756 (2006), astro-ph/0512270.

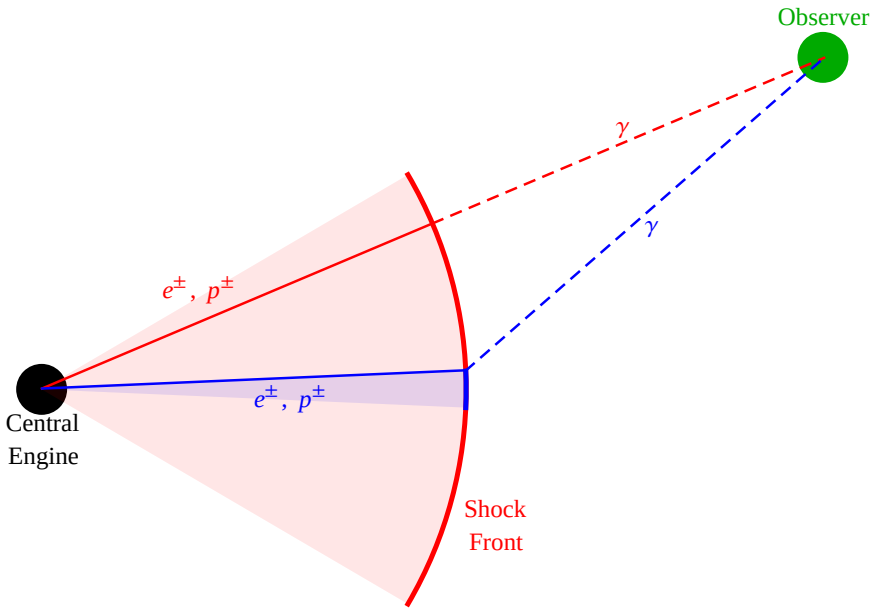


Figure 1: Model Overview. Here the red and the blue cones represent volumes through which low and high energy plasma propagates. In the case depicted the observer's off-axis angle is smaller than the opening angle of the low energy jet, so most of the observable low energy photons will travel along the straight line from the central engine (due to the relativistic beaming effect). In the same time, the observer's off-axis angle is larger that the opening angle of the high energy jet, so high energy radiation will still originate near the center of the jet (because it is the only place where there are high energy radiators). The observation time of a photon is a sum of two things: the time interval spent in plasma as a radiator (which is approximately a distance from the central engine to the point of emission); and the time interval from emission to detection (which is the distance from the point of emission to the observer's location). Given a position of the shock front, this sum is larger for high energy photons. Because of that, high energy emission will be observed later throughout the burst duration, therefore the high energy light curve will be stretched.

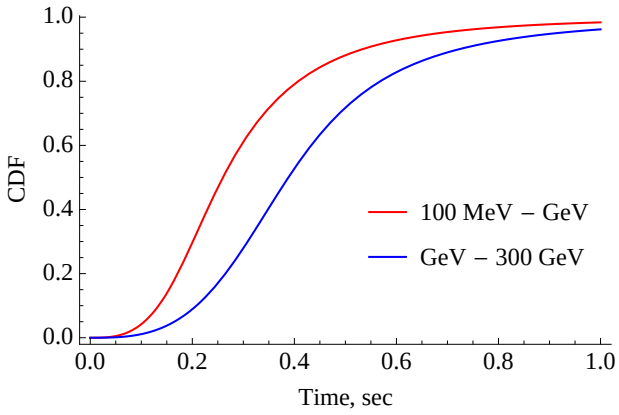


Figure 2: High and low energy light curves produced by the geometrical model. Parameter values are the same as discussed in the section 3.9. Cosmological redshift of the burst $z = 1$. Observer's off-axis angle $\chi = 0.01$.

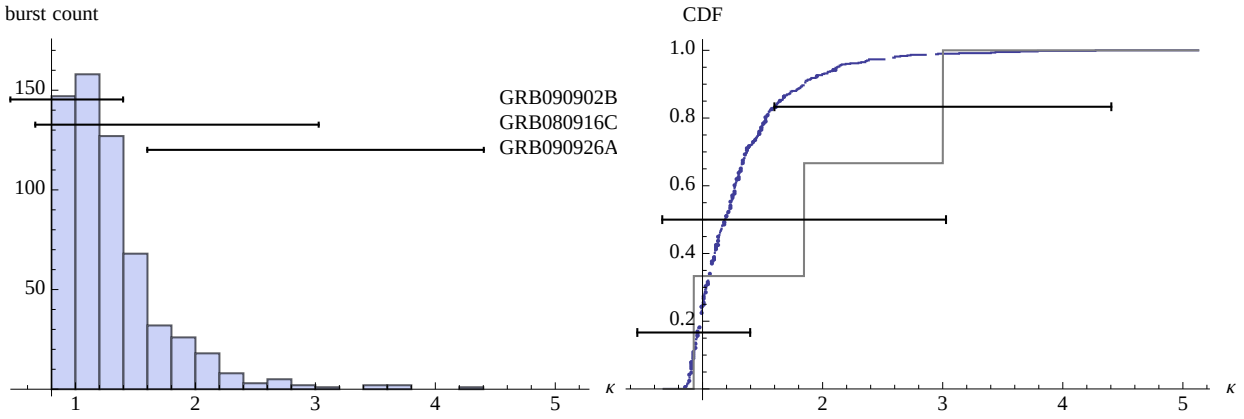


Figure 3: The histogram and the CDF of the stretching factors sample produced by our model (blue). The sample contains 600 points. The red curve is an empirical CDF of the observed sample (3 points).